Millimeter-Wave Technology for Automotive Radar Sensors in the 77 GHz Frequency Band

Jürgen Hasch, *Member, IEEE*, Eray Topak, Raik Schnabel, Thomas Zwick, *Member, IEEE*, Robert Weigel, *Fellow, IEEE*, and Christian Waldschmidt

***Abstract*—The market for driver assistance systems based on millimeter-wave radar sensor technology is gaining momentum. In the near future, the full range of newly introduced car models will be equipped with radar based systems which leads to high volume production with low cost potential. This paper provides background and an overview of the state of the art of millimeter-wave technology for automotive radar applications, including two actual silicon based fully integrated radar chips. Several advanced packaging concepts and antenna systems are presented and discussed in detail. Finally measurement results of the fully integrated radar front ends are shown.**

***Index Terms*—Automotive radar, millimeterwave silicon RFICs, packaging and interconnects, radar transceivers, antenna systems.**

I. Introduction

MAKING driving on the streets more safe and convenient has been one of the key promises for any new car generation in the last three decades. The goal is to relieve the driver from the combination of monotonic tasks and split-second decisions within complex traffic scenarios to improve safety and comfort. This functionality is nowadays called *driver assistance system*.

Table I shows a simple classification of different types of driver assistance systems. Passive driver assistance systems do not influence the vehicle motion itself, they only act on a certain scenario. Active systems however can directly influence vehicle dynamics, for example accelerating or decelerating.

Driver assistance systems require sensors that can recognize the traffic scenario around the vehicle. In order to realize these kind of driver assistance systems, sensors to recognize the traffic scenario around the own vehicle are required. Different sensor technologies such as radar, lidar, video or PMD can be used for this purpose [1], [2].

Radar can measure radial distance and velocity of remote objects very precisely. Using more than one receive or transmit channel, additional angular information can be obtained. It is also robust against environmental influences such as extreme temperatures, bad light or weather conditions. Due to these reasons, radar has been identified as the most promising technology for a number of driver assistance functions [3], [4]. Additionally, different sensing technologies can be combined together using sensor data fusion to improve the overall accuracy, reliability and flexibility of the system [5].

TABLE I
Types of Driver Assistance Systems

Passive Comfort	e.g. parking aid, where only additional information is given to the driver
Passive Safety	e.g. the airbag, where inflation is triggered only after a crash
Active Comfort	e.g. adaptive cruise control, where the vehicle actively accelerates or brakes to relieve driver of monotonic tasks
Active Safety	e.g. automatic emergency braking, where the car sharply decelerates in case of a obstacle on the road

The paper is organized as follows. Section II first gives some background information. The selection of the 77 GHz frequency band is explained and the current frequency regulation status is given. Then, the present state of the art of commercially available automotive radar sensors at 77 GHz is described using three different commercial sensors as examples.

In Section III, different application scenarios for driver assistance are introduced, each having their own requirements for the radar sensor. System parameters for three exemplary radar sensors types are given, in order to give an impression of the typical technical requirements for such sensors.

Section IV goes into more detail for the millimeter-wave frontend part of the radar sensor. It provides a description of current active components, including, the motivation behind the move to SiGe silicon semiconductor technology for the next generation of radar sensors. Different packaging concepts for millimeter-wave circuits will be shown, giving an overview of new technologies that have the potential to be used in the next generation of sensors. Section IV.C will then give an overview of antenna systems for automotive radar sensors and provides an outlook in what direction antenna systems for automotive radar sensors might evolve.

Finally, Section V presents three examples of realized radar sensors, showing actual realizations of the concepts introduced in the previous chapters.

II. Background

The first reported usage of millimeter-wave based radar technology in the automobile was in the early 1970s. A number of companies and research institutes started to look into the

Manuscript received July 01, 2011; revised November 08, 2011; accepted November 17, 2011. Date of publication January 10, 2012; date of current version March 02, 2012. This work was supported in part by the German Federal Ministry of Education and Research (BMBF) under contract 13N9820-13N9824 *Radar on Chip for Cars* (RoCC).

J. Hasch and E. Topak are with Robert Bosch GmbH, Corporate Sector Research and Advance Engineering, 70049 Stuttgart, Germany (e-mail: hasch@ieee.org).

R. Schnabel and C. Waldschmidt are with Robert Bosch GmbH, Chassis Systems Control, 71226 Leonberg, Germany.

T. Zwick is with Institut für Hochfrequenztechnik und Elektronik, Karlsruhe Institute of Technology (KIT), 76131 Karlsruhe, Germany.

R. Weigel is with Lehrstuhl für Technische Elektronik, University of Erlangen-Nürnberg, 91058 Erlangen, Germany.

Color versions of one or more of the figures in this paper are available online at http://ieeexplore.ieee.org.

Digital Object Identifier 10.1109/TMTT.2011.2178427

promise of a distance radar that could avoid collisions. First applications were devised and prototypes were built. However until 1999, due to the integration-unfriendly technology at the time, large size and high cost, no product ever made it into the market. Finally, the first generation of automotive radar sensors in the 77 GHz band became available in 1998 with the introduction of the so called *Distronic* as an option in the Daimler S class. Other companies such as Jaguar, Nissan and BMW followed in the coming years [6]. By 2003, most major car manufactures offered a radar system in their upper class segments. The application was a comfort function, where the radar sensor measures the speed and distance of the vehicle in front and automatically regulates the distance (ACC—adaptive cruise control).

Since then, several new generations of automotive radar sensors have become available from a number of manufacturers. Today's radar-based driver assistance systems have become available even for middle class cars. Accelerating this trend, a rapidly growing number of radar sensors are integrated into new vehicles, to allow driver assistance functions for comfort and safety enhancement [7].

A. Frequency Band Selection

Two different frequency bands are predominantly used for automotive radar: the 24 GHz and 77 GHz bands. Other frequencies (e.g., below 10 GHz or above 100 GHz) have also been investigated, however currently play no practical role. Naturally, there is an ongoing competition in the choice between the two frequency bands. From an engineering point of view, 77 GHz is more challenging than 24 GHz. On the other hand, the 77 GHz bands offers more opportunities to realize higher-performance sensors. An exhaustive comparison between the 24 GHz and 77 GHz band would go beyond the scope of this paper, so only a few key issues are highlighted here.

One key feature for a flexible integration of sensors into vehicles is the sensor size. The size of an automotive radar sensor is determined by the antenna aperture. Operation at 77 GHz allows a small antenna size for a given beamwidth requirement and enables good angular resolution for a small sensor size. Sensors at 24 GHz require an about three times larger aperture to achieve the same performance. For a 50×50 mm antenna aperture, using the Rayleigh criterion as shown in Section III.B with $d = 50$ mm, results in a angular separability of 17.5° at 24 GHz and 5.4° at 77 GHz. A separability of a few degrees is required for almost all mid and long range functions.

Another advantage of the 77 GHz band is that in the future short-range sensors with high spatial resolution will be introduced, having an absolute bandwidth of up to 4 GHz. This translates to a relative bandwidth of only about 5% at 77 GHz compared to nearly 17% at 24 GHz. This makes the design of antennas and wavelength dependent components much easier.

Also, the combination of high transmit power (> -40 dBm/MHz) and high bandwidth (>250 MHz) is not allowed at 24 GHz. This combination is available at 77 GHz, allowing long range operation and high distance separability at the same time.

Taking into account the recent advances in semiconductor, packaging and PCB technology, the manufacturing costs can be seen as on par between the two frequency bands. At 24 GHz, a better performance (power consumption, noise figure, performance margins) with the same technology node or usage of a different (and lower cost) technology node is possible. On the other side, the sensor at 77 GHz will typically be much smaller, reducing volume- and weight-related costs.

One widely expressed concern for 77 GHz sensors is behind-bumper integration. However, solutions to this have been investigated [8] and are thought to be feasible.

TABLE II
CURRENT REGULATION STATUS

Country	76-77 GHz	79-81 GHz
Europe (CEPT)	available	available
USA, Canada	available	discussions started
Russia	available	available
Japan	restricted to 0.5 GHz bandwidth	in discussions
China	available	-
Korea	available	-
Argentina	regulation in progress	-

B. Frequency Regulation

The operation parameters of radar sensors are not only determined by technical requirements alone. Another deciding factor is frequency regulation, governed by regulatory bodies such as the FCC in the US and CEPT in Europe. Each country can have its own regulation, sometimes conflicting with other—even neighboring—countries. Regulation is subject to constant changes, therefore only a brief overview is given.

For the operation of automotive radar sensors in the millimeter-waves, two frequency bands have emerged. One is the band from 76–77 GHz, which is available nearly worldwide. The second band is the directly neighboring band from 77–81 GHz, which has been introduced in Europe to replace ultra-wideband (UWB) automotive radar sensors in the 24 GHz band. It provides a larger bandwidth of 4 GHz instead of 1 GHz, however at reduced maximum transmit power compared to the 76–77 GHz band.

Table II shows the current regulatory status for the two frequency bands in a number of different countries. Both frequency bands are currently only available in the EU and countries associated in CEPT.

In the 76–77 GHz band, the peak transmit power is $+55$ dBm EIRP, subject to some restrictions for average power or scanning antenna systems [9]. The limits for spectral power density in the frequency band 77–81 GHz are defined in [9] and are given as -3 dBm/MHz (EIRP) maximum power spectral density, associated with a peak limit of $+55$ dBm (EIRP). Additionally, the maximum mean power density outside a vehicle is limited to -9 dBm/MHz, taking into account the additional attenuation due to mounting the sensor behind a painted bumper.

In the US, the emission limits in the frequency band 76–77 GHz are dependent on several factors (e.g., if the vehicle is moving or not). It is planned however, to harmonize the regulation with power limits similar to Europe [10].

C. Sensors on the Market

Due to the still advancing evolution of the driver assistance market and the complexity of development, there is a significant variety of implementations for automotive radar sensors in the 77 GHz band, arising from quite unique technical approaches for each manufacturer. In the following section, a brief overview on three sensor concepts that are currently available

TABLE III
COMPARISON OF RADAR SENSORS CURRENTLY ON THE MARKET

Parameter	Bosch LRR3	Conti ARS 300	Denso DNMWR004
Dimensions	74x70x58 mm	120x90x49 mm	78x77x38 mm
Max. detection range	250 m	200 m	150 m
Horizontal FoV	30°	58°/17°	20°
Number of beams	4	15/17	5
Beamsteering	Fixed-beam	Mechanical	Electronic
Multirange capability	Single	Multi	Single

on the market will be given with their key performance indicators being illustrated in Table III. Their main differentiating factor is the target angle estimation, resulting in a use of different beam steering techniques. Despite those different approaches, all presented sensors rely on the FMCW modulation technique.

The LRR3 sensor by Bosch [11] has been available since 2009. Its most prominent feature is the dielectric lens antenna that provides the high gain to achieve the maximum distance of 250 m. It is the only example in this field not scanning its field of view. To achieve angular information in the azimuthal plane, it uses four patch antennas placed in the focal line of the dielectric lens to create four slightly offset beams. All four antennas are receive antennas with the middle two antennas also simultaneously transmitting. Using phase and amplitude information of all four channels, angular information of detected objects can be determined. The sensor was the first to use SiGe integrated circuits at 77 GHz. The SiGe chip is mounted on a multilayer PCB and wire bonded to an RF substrate on the top side of the PCB. The patch antennas to illuminate the antenna are also placed on the RF substrate. The sensor is described in more detail in Section V.A.

The ARS 300 presented by Conti [12] in 2009 mechanically scans the field of view. It uses a grooved rolling spindle to create a narrow scanning antenna beam [13]. By using different patterning of the spindle, the sensor can switch between long and mid range mode, changing its field of view. By pivoting a reflector plate, the antenna can scan in multiple levels of elevation allowing auto-alignment operation. The antenna is fed by a RF module comprising multiple GaAs MMICs for RF generation and a balanced mixer with discrete diodes.

Denso's third generation long range radar [14] was introduced in 2008 and utilizes digital beamforming (DBF) using one transmit antenna and a five switched receive antennas. By serially switching to the different receive antennas, the electronics for only a single receiver channel needs to be implemented. The antenna itself is realized as a slotted waveguide array and uses a three-dimensional waveguide network to distribute the antenna channels to the RF module. The transmitter is realized using four GaAs MMICs and the receiver uses three additional MMICs. The complete RF module is encapsulated in a ceramic package.

III. REQUIREMENTS

With the growing penetration of driver assistance systems in the market, an increasing list of functions are being addressed based on radar sensors [15], [16]. Such functions include comfort improvements like adaptive cruise control (ACC), where the vehicle supports the driver by automatically adjusting the speed depending on preceding vehicle and even decelerating to a total stop in case of a traffic jam. Additionally, safety-related

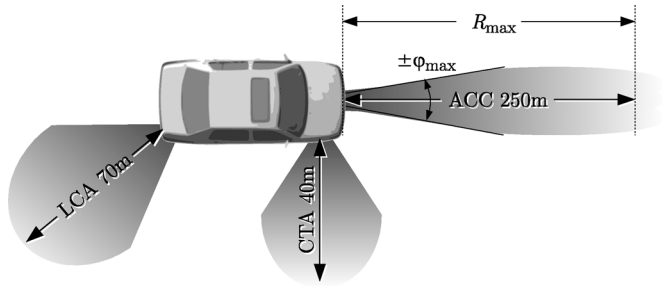

Fig. 1. Field of view and distance range for three exemplar functions.

TABLE IV
SENSOR CLASSIFICATION

Type	LRR	MRR	SRR
Maximum transmit power (EIRP)	55 dBm	-9 dBm/MHz	-9 dBm/MHz
Frequency band	76-77 GHz	77-81 GHz	77-81 GHz
Bandwidth	600 MHz	600 MHz	4 GHz
Distance range $R_{\min}...R_{\max}$	10-250 m	1-100 m	0.15-30 m
Distance resolution ΔR	0.5 m	0.5 m	0.1 m
Distance accuracy δR	0.1 m	0.1 m	0.02 m
Velocity resolution Δv	0.6 m/s	0.6 m/s	0.6 m/s
Velocity accuracy δv	0.1 m/s	0.1 m/s	0.1 m/s
Angular accuracy $\delta\varphi$	0.1°	0.5°	1°
3 dB beamwidth in azimuth $\pm\varphi_{\max}$	±15°	±40°	±80°
3 dB beamwidth in elevation $\pm\vartheta_{\max}$	±5°	±5°	±10°
Dimensions	74x77x58 mm	50x50x50 mm	50x50x20 mm

functions begin to appear, supporting the driver in critical situations. Examples are lane change assistant (LCA), watching for traffic when starting overtaking action or cross traffic alert (CTA), warning of approaching vehicles at a junction. Fig. 1 graphically depicts the field of view of the radar sensor for these three example functions. The field of view here is defined as having a maximum measurement distance $R_{\max}$ and the angular range $\pm\varphi_{\max}$.

A. Classification

Looking at Fig. 1 it can be easily understood that for each individual function a different sensor specification is needed. This can lead to an intractable number of different radar sensor specifications, each designed to address the appropriate distance range and field of view.

To simplify the following technology assessment, only three generic sensor types will be considered here.

- LRR—Long Range Radar
  for applications where a narrow-beam forward-looking view is required, like ACC
- MRR—Medium Range Radar
  for applications with a medium distance and speed profile, like CTA
- SRR—Short Range Radar
  for applications sensing in direct proximity of the vehicle, like obstacle detection and parking aid

In Table IV, technical system parameters for these three generic sensor types are given.

Fig. 2 depicts the range and angular resolution definition. The range resolution ΔR is defined as the ability to distinguish between two targets in radial distance, while the angular resolution

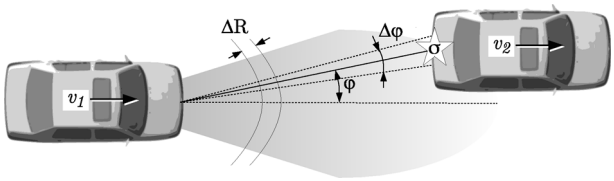

Fig. 2. Range resolution and angular resolution.

$\Delta\varphi$ defines ability to distinguish two targets by angle. It should be noted, that the measurement accuracy (δR for range, δv for velocity and $\delta\varphi$ for angle) describes the amount of uncertainty that exists in the measurement and can be much smaller than the corresponding resolution.

One of the main challenges for an automotive radar sensor is the separation of targets with a small radar cross section, such as a motorbike, and targets with a large radar cross section, such as a truck, traveling at nearly the same distance and velocity in adjacent lanes. This discrimination can be achieved by high resolution and dynamic range in at least one of the measurement quantities distance, velocity or angle.

B. Measurement Quantities

A generic bistatic radar system with separate transmit and receive antennas consists of a transmitter with the transmit power P_{T} and the antenna gain G_{T} and the receiver with the antenna gain G_{R} and the received power P_{R} from a target with the radar cross section σ.

For this basic bistatic scenario, the well-known radar equation [17] specifies the power density $p(R)$ illuminating a target in the distance R:

$$p(R) = \frac{P_{\mathrm{T}} G_{\mathrm{T}}}{4\pi R^2} \tag{1}$$

For a given radar cross section σ, the receive power P_{R} at the radar receiver can then be calculated to:

$$P_{\mathrm{R}} = \frac{P_{\mathrm{T}} G_{\mathrm{T}} G_{\mathrm{R}} \lambda^2}{(4\pi)^3 R^4 L}\sigma \tag{2}$$

Here, the factor $L < 1$ denotes the combined losses within the radar sensor.

The signal-to-noise ratio can then be calculated as:

$$S/N = \frac{P_{\mathrm{R}}}{P_{\mathrm{N}}} \tag{3}$$

The noise power P_{N} in the baseband comes from a number of noise sources, including thermal noise, receiver noise figure, bandwidth, amplitude and phase noise of the oscillators and $1/f$ noise. The threshold S/N for target detection is typically 10 dB. This threshold value has shown to give a low false alarm rate with a good probability of detection.

As the receive and transmit antennas are very close to each other, the radar cross section σ can be approximated as a monostatic radar cross section [18]. Fig. 3 shows the monostatic radar cross section of a car (Mazda 6) measured at 77 GHz [19]. Four maxima can be seen at the four sides of the car, exceeding a value of $\sigma = 30$ dBsm. In a real traffic scenario, a vehicle needs to be characterized by more than one single radar cross section. It can be typically characterized as a number of separate scattering centers [20].

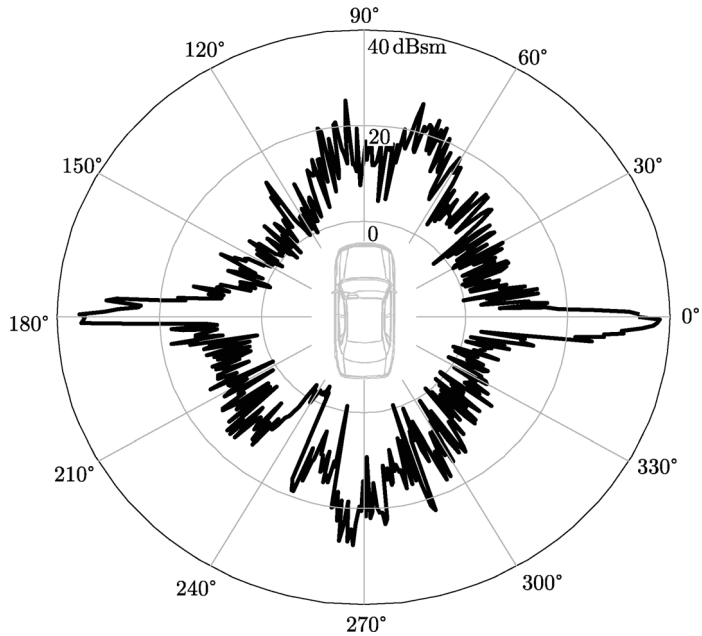

Fig. 3. Measured monostatic RCS of a vehicle.

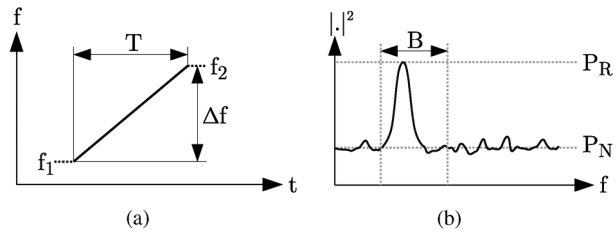

Fig. 4. FMCW Modulation. (a) Frequency characteristics, (b) Baseband signal.

For the following discussion of the radar performance parameters, linearly swept frequency modulation (FMCW) is assumed, as shown in Fig. 4.

In Fig. 4(a) the frequency sweep with $\Delta f = f_2 - f_1$ in time duration T is depicted. This leads to a baseband signal shown in Fig. 4(b), where a target is mapped to a beat frequency f_b. The beat frequency f_b at the receiver can be calculated to

$$f_b = \frac{2R\Delta f}{cT} + f_d \tag{4}$$

where the velocity difference $v = v_1 - v_2$ between the two vehicles of Fig. 2 leads to a doppler frequency f_d

$$f_d = \frac{2v}{\lambda}\cos\varphi \tag{5}$$

In (4), range R and velocity v are coupled. In order to separate these two quantities for multiple targets, multiple FMCW sweeps with different ramp slopes $\Delta f/T$ have to be performed.

An important performance criterion is the resolution or separability of speed and distance between two targets. From [21], the distance resolution ΔR and velocity resolution Δv can be calculated with

$$\Delta R = \frac{c}{2\Delta f} \tag{6}$$

$$\Delta v = \frac{\lambda}{2T} \tag{7}$$

The accuracy of the measurement is characterized by the rms measurement error δ. It is mainly determined by the linearity error and the signal-to-noise ratio S/N. Using the signal-to-noise ratio (S/N), the accuracy can be given as

$$\delta R_{\mathrm{SNR}} = \frac{\Delta R}{\sqrt{2S/N}} \tag{8}$$

$$\delta v = \frac{\Delta v}{\sqrt{2S/N}}. \tag{9}$$

A frequency error δf due to a nonlinear frequency sweep leads to a distance error δR_{NL} [22]

$$R_{\mathrm{NL}} = R_{\max} \cdot \frac{\delta f}{\Delta f}. \tag{10}$$

The combined distance measurement accuracy is then

$$\delta R = \sqrt{(\delta R_{\mathrm{SNR}})^2 + (R_{\mathrm{NL}})^2}. \tag{11}$$

Another important measurement quantity is angular information of the target in azimuth and elevation. System concepts to enable angular measurement are discussed in Section IV-C. Here, only the basic requirements for angular resolution and accuracy are discussed.

The angular resolution [23] using the Rayleigh criterion can be calculated

$$\Delta\varphi = 1.22\frac{\lambda}{d} \tag{12}$$

where d is the size of the aperture of the antenna in the direction considered. The angular accuracy can again be given like before, if only the signal-to-noise ratio is considered

$$\delta\varphi = \frac{\Delta\varphi}{\sqrt{2S/N}.} \tag{13}$$

IV. Millimeter-Wave Frontend

The millimeter-wave frontend of an automotive radar sensor still changes quite a lot in each new generation. It is very much technology driven, as new solutions in semiconductor technology, packaging technology and antenna systems become available. For semiconductor technology, higher performance, more integration and lower power consumption are key factors.

A. Active Components

For the active components of the millimeter-wave frontend, the available semiconductor technology is the key enabler. Higher performance, more integration and lower power consumption at low cost are the key requirements here.

1) Semiconductor Technology Selection: The first commercially available automotive radar sensors in the 77 GHz band that emerged on the market beginning in 1999, typically used GaAs Gunn diodes mounted inside a waveguide cavity, as millimeter-wave signal source and discrete Schottky diodes flip-chipped on quartz glass substrate with thin film patterning [6], [24].

Since this first generation of sensors, the available technology has improved and costs have decreased significantly. Discrete semiconductor components have been replaced by MMIC blocks or even complete transceiver circuits.

TABLE V
SiGe Process Foundries and IDMs

Parameter	Unit	IBM	TowerJazz	IHP	STM	Freescale	NXP	IFX
Process		8HP	SBC18H3	SG13S	B9CMW	HiP6MW	QUBiC4Xi	B7HF200
CMOS node	nm	130	180	130	130	180	250	350
npn f_T	GHz	200	240	250	230	185	216	200
npn f_{max}	GHz	265	260	300	290	260	177	250
npn β		450	na	900	950	425	2700	1000
npn BV_{CE0}	V	1.7	1.2	1.7	1.5	2.0	1.44	1.5
Metal layers	#	4Cu, 2Al	Al	6 Al	6 Cu	5 Cu	6 Al	4/6 Cu
MIM capacitor	ff/µm²	2	2	1.5	2	1.6	5	1.4
Varactor pn		yes	yes	no	yes	yes	yes	yes

Mature chip sets in GaAs technology are reported from semiconductor manufacturers UMS [25] and TriQuint [26]. Additionally, a number of radar sensor implementations using GaAs MMIC have been reported in the literature, recent examples are [27], [28], and [29].

However, at 77 GHz, GaAs is on the verge of being replaced in the next generation of products by most manufacturers, as silicon-based SiGe technology has become a viable and cost-effective approach. The RF performance of modern SiGe processes has been demonstrated by a number of research groups [30]–[32] using semiconductor technology from manufacturers such as Freescale [33], TowerJazz [34], ST Microelectronics [35], IBM [36] and Infineon [37]. Infineon and Freescale have complete transceivers using their own flavor of SiGe technology [38], [39]. Infineon's radar transceiver has been in mass production in the LRR3 radar sensor since 2009 [11]. Table V gives an overview over the currently available SiGe processes available at foundries or independent device manufacturers (IDM). They typically provide $f_{\max}$ frequencies of well over 200 GHz for npn transistors. All provide additional CMOS transistors, which allows easy integration of digital circuitry with the exception of Infineon, which currently has a bipolar-only process. Higher ambient temperatures decrease f_{T} and $f_{\max}$ considerably. At 125°C a reduction of at least 20% compared to 25°C was found [40]. According to [41], $f_{\max}$ should be at least 2 times the operating frequency for an amplifier, so the required room-temperature $f_{\max}$ is 200 GHz at minimum. In [42], the influence of temperature on the performance of W-band circuits was investigated in detail.

Recently, the first implementations of highly integrated 77 GHz radar transceivers in pure CMOS, using 90 nm and 65 nm nodes, have been published [43]–[45]. They demonstrate the technical feasibility of realizing such a system. However, there are still a number of obstacles to be overcome, until a true automotive grade radar sensor for the applications discussed in this paper, can be realized. From a technical side, achieving the required output power, dynamic range and linearity is still not proven. A good comparison of the differences between SiGe and CMOS can be found in [46].

Additionally the required temperature range of -40 to $+125°\mathrm{C}$ ambient especially for the power amplifier still is problematic, as can be seen in [47]. It is even possible, that output power and temperature performance may always be limited, as shown in [48].

Since the main driver to CMOS is integration, it is unclear how a highly integrated radar system can look like. There are

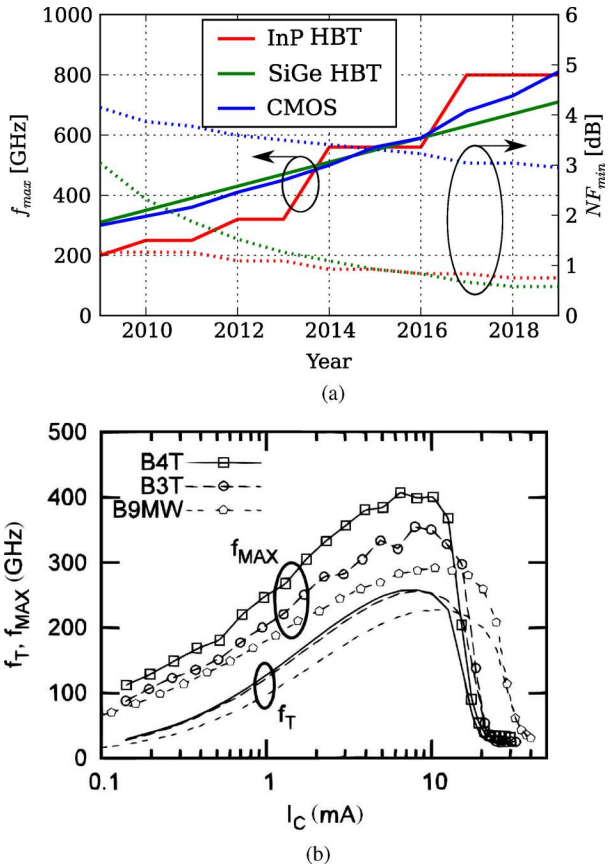

Fig. 5. Semiconductor performance trends. (a) Trend projected by ITRS for transistor speed and noise figure, (b) $f_{\max}$ vs collector current for a SiGe bipolar transistor.

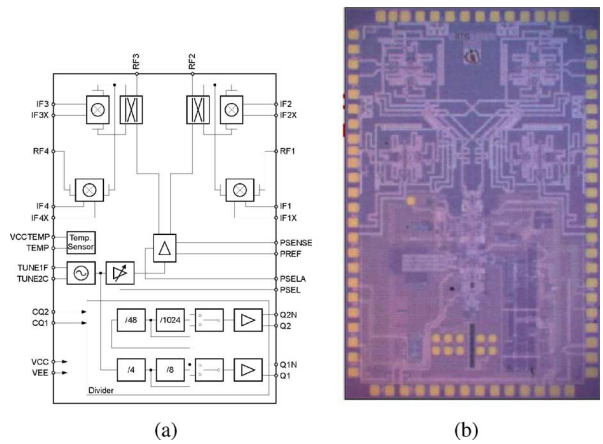

Fig. 6. Four channel transceiver chip [38]. (a) Block diagram, (b) Chip micrograph.

many very different implementations, and, as shown in [49], the design costs for modern CMOS processes are expected to drastically increase due to complexity of the circuits and the highly advanced design tools required. In the coming years, new high volume applications for radar sensors might emerge, justifying the high one-time costs for developing a CMOS solution [49] while living with the reduced system performance due to the impediments described above. For now, SiGe technology in its BiCMOS flavor is destined to be the mainstream semiconductor technology for automotive millimeter-wave radar in the next years.

Fig. 5 tries to give some insight into the future. In Fig. 5(a) the projected ITRS trend [50] for three different semiconductor technologies is shown. It can be seen that for InP, SiGe and CMOS technology the transistor speed will continue to increase rapidly and the noise figure at 77 GHz will decrease further. For a radar sensor, this translates to lower overall noise figure (oscillator phase noise, mixer and LNA noise) and allows a reduced transmit power. In Fig. 5(b) the evolution for the f_{T} and $f_{\max}$ of a SiGe process is shown [51]. For a required given transistor speed, the biasing current can be greatly reduced, leading to much reduced power consumption.

2) Examples: In this subsection, two millimeter-wave chips are introduced. The first chip shown in Fig. 6 is a four channel radar transceiver implemented in Infineon's B7HF bipolar SiGe technology and has been presented in [38]. Fig. 6(a) shows the block diagram of the transceiver. It consists of a fundamental 77 GHz VCO with frequency divider stages for frequency stabilization, a four channel receiver with two of the channels operation simultaneously as transmit/receive channel. Each of the transmit channels provides an output power of 7 dBm. The transmit channels can be selected by a simple one-mask change, so different versions of radar sensors can be built with the same basic transceiver. Some key figures of the transceiver is a noise figure of 17.7 dB (23.4 dB for transmit/receive channels) and a receiver gain of 14.2 dB. The input match, important for simultaneous transmit/receive operation, is better than 20 dB for the receive-only and better than 12 dB for transmit/receive channels. The transceiver operates at 5.5 V and has a power consumption of less than 4 W. It is used in the LRR3, which is described in Sections II.C and V-A. The chip size is 3.25×2.1 mm.

Two key components for a FMCW radar will be investigated further in the next paragraphs, the mixer and the frequency generation circuit.

Mixers play a major part in determining the performance of a radar receiver. Linearity, conversion gain, noise figure and power consumption are the most important parameters. Assuming an output match to off-chip components of 20 dB, the mixer will receive $-16\ \mathrm{dBm} = 7\ \mathrm{dBm} - 20\ \mathrm{dB} - 3\ \mathrm{dB}$ (3 dB have to be subtracted for the receiver/transmit coupler) the RF input. Close-by objects in close proximity to the antenna could lead to even higher values. This contributes to one of the main problems of an FMCW radar, the DC offset at the output of the mixer. This offset has to be taken into account in the following signal processing stages.

Using (2), for an object at 250 m distance with the parameters of a long range radar (LRR) system from Table IV a receive power of -100 dBm can be calculated. In order to achieve a dynamic range in the order of 90 dB or more, the mixer core will typically be biased with a high current. This works against the low-power requirement. The currently dominating mixer architecture is the Gilbert type mixer because it offers a good suppression of unwanted intermodulation products [52]. Usually the Gilbert mixer core is amended by filter circuitry and buffers to provide better port isolation and impedance matching. Recent publications report improved power consumptions figures while retaining the required performance [53].

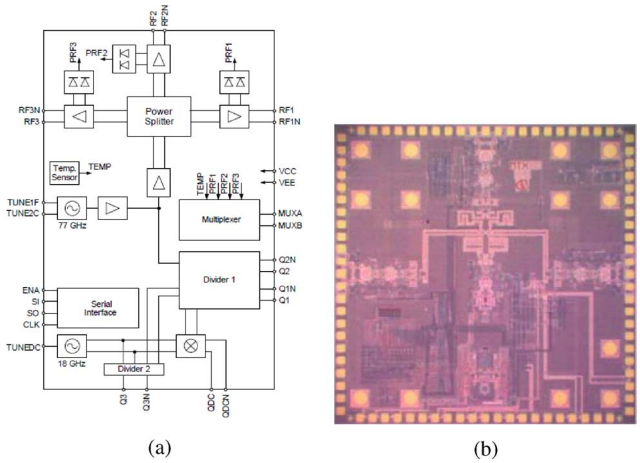

Fig. 7. Three channel transmitter chip. (a) Block diagram, (b) Chip micrograph.

The performance of the frequency source is another key performance figure. The millimeter-wave signal is generated by a fundamental 77 GHz VCO. The linear FMCW modulation is applied off-chip using the integrated frequency divider to drive a PLL circuit. The phase noise of the VCO was measured to -75.3 dBc/Hz@100 kHz at 25°C. This number is not sufficient for long-range operation, as the noise skirts of the oscillator signal can mask weak signals [54]. In order to improve the phase noise performance, the divided-by-four VCO signal can be mixed down using an additional low-phase noise 19 GHz oscillator [55], rather than divided down to the low-GHz frequency range which is suitable for the PLL circuit.

An example of the next generation of circuits is shown in Fig. 7. It shows a three channel transmitter, developed for use in a bistatic radar sensor. It consists of a 77 GHz fundamental VCO, again with attached frequency dividers for frequency stabilization. Also, an additional 18 GHz VCO has been added, to enable the direct down-conversion of the divided-by-4 77 GHz signal instead of using high divider ratios in order to improve phase noise. Each output channel can be individually turned on and is equipped with a power sensor that is able to monitor the transmitted and reflected power and provide them to an external surveillance circuit using an analog multiplexer. An integrated 19 GHz downconverter and two divider chains can be used for PLL operation.

A digital control interface allows to configure the chip, e.g., divider ratio settings and output channel power control. Beside its higher functionality the chip is more efficient due to e.g., a lower required supply voltage of 3.3 V, resulting in a power consumption of $P_{\mathrm{DC}} \approx 2$ W. The chip size is 3×3 mm.

B. Packaging

Another crucial element in a low-cost millimeter-wave frontend is the packaging technology. Traditionally wire-bonding and flip-chip packaging have been used for microwave and millimeter wave transitions to transfer signals off-chip. After a brief review of these two established technologies, new developments will be presented.

Important parameters are losses and reflections in the transition from chip to substrate, thermal conductivity to dissipate the heat coming from the active circuits, reliability, flexibility and cost.

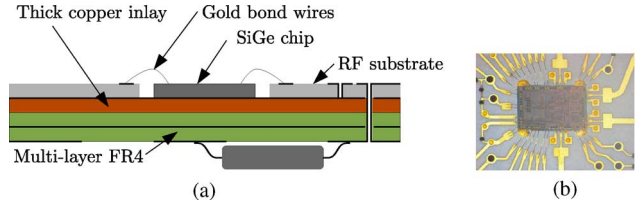

Fig. 8. Chip on board wire bonding. (a) Cross section of a PCB with a wire bonded SiGe chip, (b) SiGe transceiver bonded to RF substrate.

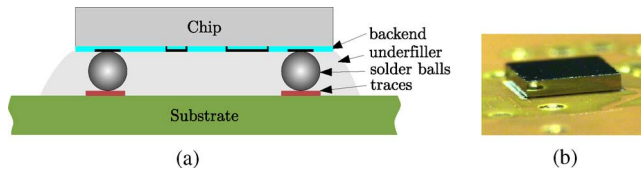

Fig. 9. Flip chip mounting on substrate. (a) Cross section of flip-chip mount, (b) Photo of mounted chip.

1) Chip on Board: Wire bonding is by far the most used technology to connect a semiconductor chip to a printed circuit board. A typical setup is shown in Fig. 8(a). The chip is mounted in a cavity to avoid height differences for the bond wires. To achieve a good heat dissipation, the chip is mounted directly on a thick copper inlay. The top side of the PCB is laminated with a RF substrate to achieve low signal losses and allow the realization of antenna structures. On the bottom side, multilayer FR4 is used and standard electronic components can be mounted.

Fig. 8 shows a close-up view of a SiGe transceiver chip mounted on such a PCB board. The millimeter-wave signals are single-ended, therefore an additional ground signal bond wire is placed at each side.

At millimeter-wave frequencies, the parasitic electrical properties of the bond wire can severely effect the performance of such a transition. Although an optimized geometry of wire-bond and matching structures can achieve good performance, the wiring tolerances in mass production are significant and can be up to $\pm 15\%$. A detailed analysis of this setup was performed in [56] and showed reflections of up to -10 dB. Losses can reach up to 2 dB due to mismatch and radiation [57]. Measurements in [58] show a return loss better than 12 dB and insertion loss less than 0.3 dB in the frequency range of DC to 80 GHz.

2) Flip-Chip: As an alternative to wire bonding, flip-chip packaging, as shown in Fig. 9, is also being used. An overview of millimeter-wave flip-chip technology is given in [59]. It can deliver a better RF performance with reduced radiation losses and improved matching. Due to the smaller electrical length and mechanical tolerances, a more consistent performance and more broadband operation can be achieved. Another advantage of flip-chip packaging is the more flexible distribution of contact pads within the chip, allowing a more relaxed placing and routing to off-chip circuitry. An example of the millimeter-wave performance for a flip-chip transition can be found in [60], where an insertion loss less than 0.2 dB and a match better than 20 dB up to 82 GHz was reported.

Apart from the required fine line/space requirements for the substrate the chip will be mounted on, detuning due to the close proximity to a substrate or underfiller, the worse thermal contact and the fine line pitch on the substrate can be mentioned.

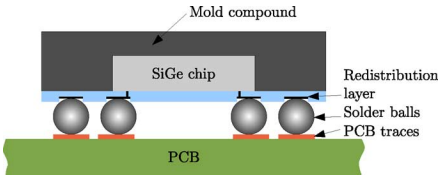

Fig. 10. Cross-section drawing of an eWLB package.

For GaAs chips, a concept using hot vias through the bulk of the chip was reported in [25]. This enables better thermal conductivity and reduces the detuning effect, while still retaining the good performance of a flip-chip transition.

3) eWLB Package: An important driver in packaging technology is the "interconnect gap" that characterizes the pitch and pad size for chips shrinking faster than the line/space structure capabilities of PCB technology. Therefore, interposers or redistributing layers have been added to reduce the requirements on PCB technology.

This is the basic idea of the eWLB (embedded wafer level BGA) package, which was introduced in 2006 by Infineon for their mobile phone chipsets [61]. Very similar approaches have been developed by other companies and have been in mass production for several years. A cross section drawing of an eWLB package is shown in 10.

To use this package for 77 GHz circuits, a number of obstacles had to be overcome. As the chip is now facing the PCB with its active side, the electrical function can be influenced by the PCB and by the solder balls. Solder balls therefore could not be allowed in most areas of the chip and need to be moved to the mold compound area. Also, the heat transfer between the chip and the PCB is now mostly due to the solder balls.

As the mold compound exhibits low losses ($\tan\delta = 0.004$), low-loss coplanar lines can be realized. Measurement results of transmission lines show insertion losses of 0.2 dB/mm at 60 GHz compared to on-chip components and a Q-factor of up to 39 for spiral inductors [62]. Furthermore, the results of the first fully operational 77 GHz SiGe mixer implemented in an eWLB package show a conversion gain of only 1 dB below on-wafer measurement [63].

Due to different coefficients of thermal expansion (CTE) between chip and mold compound, mechanical stress can occur, leading to warpage. In addition it has been revealed that solder ball fatigue is the dominating failure mode [64], [65] which is related directly to the distance between solder ball and package's neutral point.

The eWLB package also offers compatibility to both side-by-side and stacked 3-D layouts by using RDL interconnection as well as through silicon vias (TSV) and through mold vias (TMV) [64], [66], making the package an excellent starting point for future developments.

4) Antenna in Package: All of the packaging solutions presented so far still rely on an additional millimeter-wave low loss substrate to distribute the RF signal to the antenna or to realize the antenna directly on the substrate. Integrating the antenna in the package allows avoiding any transition of the millimeter-wave signal from the package to a PCB board, reducing costs for the PCB significantly. In our approach, the the antenna was realized using the eWLB package introduced in the previous section.

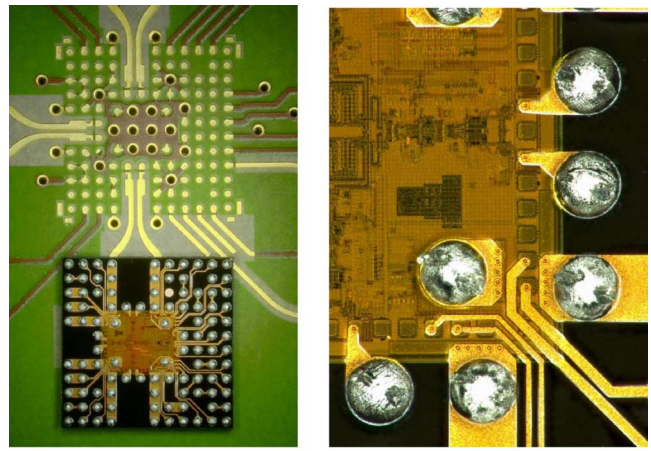

Fig. 11. Photographs of eWLB package and PCB footprint. (a) eWLB package and PCB, (b) close-up view.

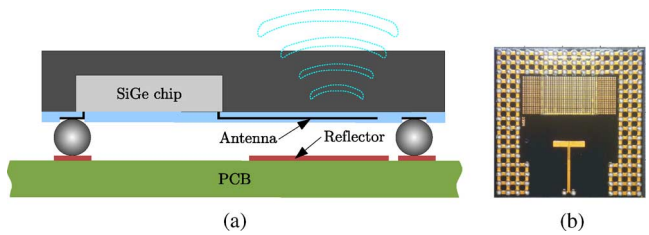

Fig. 12. Antenna integrated in eWLB package concept. (a) Cross section drawing, (b) Photo of eWLB bottom side with dipole element.

Fig. 12(a) shows a cross section drawing of package-integrated antenna [67]. The antenna element is realized using the redistribution layer of the package and radiates through the low-loss mold compound. To improve directivity, a metallic patch is added on the PCB below the antenna element, functioning as reflector.

In Fig. 12(b), the photo of a realized antenna is shown. The package size is 8×8 mm and contains a differentially fed dipole antenna with a length of about 1.65 mm, realized on the redistribution layer. For testing, a chip is also integrated in the package, the antenna however is fed using a differential transition at the edge of the package. The antenna has a gain of 5 dBi over a half-power beamwidth of $\pm 45°$ in the E-plane and $\pm 60°$ in the H-Plane.

More antenna elements can be realized in the package, so group antennas with higher gain or antennas for multiple channels can be realized. However, because of the mechanical properties of the eWLB package described in the previous section, the maximum size of the eWLB severely limits the number of antenna elements.

5) Antenna on Chip: Taking antenna integration even one step further leads to the realization of the antenna directly on the chip. However, the radiation efficiency of an on-chip antenna is typically quite poor, as most of the energy is dissipated in the low-resistivity silicon. Adding a thick dielectric layer on top of the chip [68] or using micromachining techniques ([69]) are the possible solutions to increase the antenna efficiency. These approaches require an additional processing of the complete wafer and are often difficult in handling and processing. Also, due to

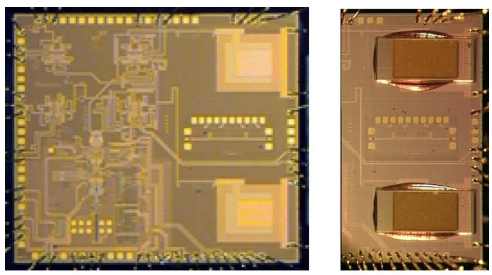

(a) (b)

Fig. 13. Antenna on chip transceiver micrographs. (a) Chip without mounted quartz glass resonators, (b) Quartz glass resonators.

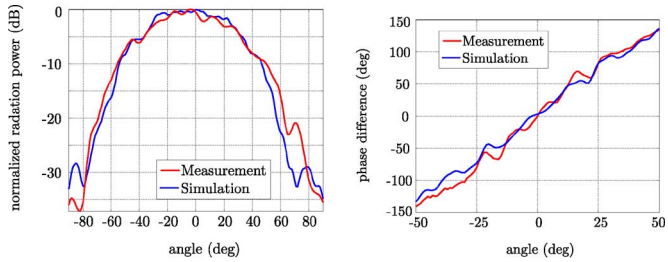

(a) (b)

Fig. 14. Performance of the on-chip antenna. (a) Normalized antenna pattern, (b) Phase difference between the two channels.

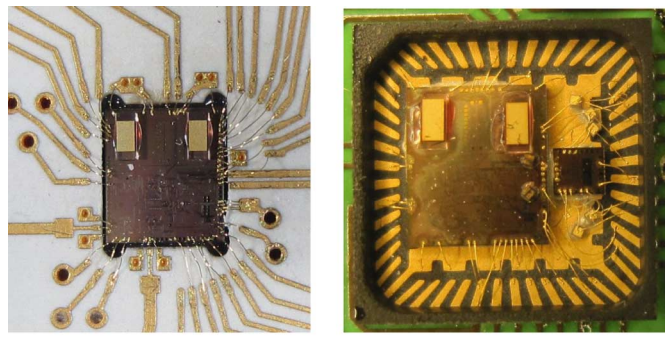

(a) (b)

Fig. 15. Comparison of SiGe transceiver chip mounting. (a) Bonded in PCB, (b) Mounted in QFN package.

material parameter tolerances, they are often not suitable for mass production.

As an alternative approach, parasitic resonators can be placed above an on-chip antenna element, leading to a significantly improved antenna performance by coupling the electromagnetic wave from the chip to the resonator [70], [71]. This technique requires no further processing of the silicon wafer and can be easily automated in production using standard packaging equipment.

In order to investigate the proposed on-chip antenna concept and verify its performance, the four channel radar transceiver introduced in Section IV-A.2 was used and two on-chip antenna elements were added to the transmit/receive channels. The remaining two receive-only channels are not used. A micrograph of the realized circuit is shown in Fig. 13(a).

The on-chip antenna elements are based on shorted quarter-wavelength microstrip lines, formed by the top and bottom metal layers of the backend. The microstrip line acts as a patch antenna with one radiating slot. The resonant frequency of the antenna is mainly determined by the length of the line. Due to the thin substrate between the ground plane and the patch element in the 10 μm range, most of the radiation would be dissipated due to conductor and dielectric losses, resulting in a low antenna efficiency of less than 10%.

The parasitic resonator realized as $\lambda/2$ long thin-film metal patch on top of a $1.3 \times 0.6 \times 0.25$ mm quartz glass. It is positioned directly above the on-chip patch antenna element and drastically improves the antenna efficiency and bandwidth. Fig. 13(b) shows the chip with the quartz glass mounted.

The two on-chip antennas are spaced at $\lambda/2$ distance to allow direction of arrival (DOA) estimation of a target detected by the radar or provide two separate antenna beams used for illuminating an additional dielectric lens that will be presented in Section IV-B.5. The antenna pattern and phase difference between the two receive channels for a single target is shown in Fig. 14. The ripple on both graphs is due the influence of the bondwires and reflections in the housing used in the measurement setup.

In the setup presented in [70], the radar transceiver chip was glued on an aluminium heatsink and connected to a surrounding high-frequency PCB using gold wire bonds, see Fig. 15(a). An additional 19 GHz DRO downconverter MMIC [55] was used to achieve a good phase noise behavior of the 77 GHz signal. To benefit from a low-cost PCB technology, an SMD realization has been employed using the same transceiver MMIC with integrated antennas. In this setup, the millimeter-wave transceiver chip was placed together with a new bare die 19 GHz VCO downconverter MMIC [72] into a 7×7 mm open-cavity QFN package as shown in Fig. 15(b). The chip pads were contacted to the QFN package using gold wire bonds.

C. Antenna System

As described in Section II.C, the antenna system is one of the main differentiating factors of a radar sensor. Based on the standard antenna performance parameters such as gain, input match, bandwidth or the number of channels, it defines the field of view and achievable angular object separation of a radar system. The antenna system therefore not only comprises of the radiating structure, it also defines how the desired properties in the angular domain are achieved. These properties are becoming even more important for the next generation of automotive radar sensors [3]. Four antenna system concepts will be briefly discussed below to motivate further developments in the antenna system domain.

1) Quasi-Optical Beamforming: This beamforming concept uses quasi-optical elements like a dielectric lens to shape the antenna pattern and obtain a fixed field of view. Examples of quasi-optical beamforming antennas are the LRR3 using a dielectric lens antenna [73] (as shown in Section V-A) or a folded reflector antenna [74]. Typically, this approach is used for a long-range operation, where a narrow field of view is required. With this concept, a large antenna aperture at low cost can be achieved, as quasi-optical elements can often be mass produced easily. If more than one antenna feed is used, an offset between

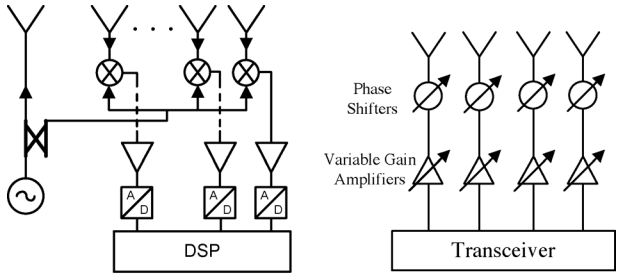

Fig. 16. Analog and digital beamforming concepts. (a) Digital beamforming system, (b) Phased array system.

TABLE VI
COMPARISON OF ANTENNA SYSTEM CONCEPTS

Parameters	quasi-optical beamforming	digital beamforming	analog beamforming	mechanical scanning
Field of view	narrow	wide	wide	very wide
Simultaneous multiple beams	yes	yes	no	no
Antenna scanning rate	continuous	continuous	fast	slow
Interference suppression	high	low	high	high
Required signal processing power	medium	high	small	small
Manufacturing complexity	easy	medium	medium	hard

the different feeds allows the generation of simultaneous or sequential multiple beams looking in different directions. However, a wide field of view and a narrow antenna beamwidth are not easy to obtain at the same time [75].

If each antenna feed is connected to an individual receiver channel, parallel data acquisition can be achieved, allowing processing of multiple antenna beams simultaneously. Monopulsing can be used to gather angular information of a detected object using multiple antenna beams [76].

2) Digital Beamforming (DBF): In this configuration, the beamforming is carried out in the digital baseband. The concept from [77] is shown Fig. 16(a). To achieve a narrow beamwidth and high angular resolution, typically eight or more channels need to be provided. For this large number of channels, there is a significant cost penalty. As one approach to reduce the number of receivers, a switch in the millimeter-wave path can be added, so only one receiver channel is needed [78]. Multipath effects and interfering signals are also processed in the digital baseband, therefore the receiver requires sufficient dynamic ranges to process these interferences. Although DBF systems are mostly used on the receiver side, they can also be implemented on the transmitter side [79], [80].

Since the beamforming is performed in the digital domain, this concept provides a high degree of flexibility. The calibration is also straightforward since all receiver channels are identical and have fixed properties.

3) Analog Beamforming: Analog beamforming refers to the technique where switchable or steerable antenna patterns can be generated directly in the millimeter-wave frontend. Numerous millimeter-wave antenna concepts can be categorized within this beamforming network. The most popular and common ones for analog beamforming are phased arrays with phase shifters [81], [82], as shown in Fig. 16(b). By controlling the phase weights of each phase shifter electronically, the direction and beamwidth of the antenna can be adjusted to a desired value almost instantaneously. This property provides multi-mode ability via beam shape versatility. By providing variable gain for each channel, the sidelobe levels can be kept low.

Until the last decade, the use of the phased array concept for the automotive radars was almost impossible due to high cost of millimeter-wave phase shifters. However, improved silicon semiconductor technology allows the integration of multiple channels of phase shifters and variable gain amplifiers on a single chip [83].

Phased arrays can be classified into three different architectures, depending on the location of phase shifters or switches (RF, IF and LO phase shifting) [83]–[85]. Among these, RF phase shifting is the most common and widely used phased array system, usually used for the military and satellite communication radars [86]. Analog beamforming can have high interference suppression in the analog path.

4) Mechanically Scanned Array: Mechanical scanning is a well-proven approach to achieve high angular resolution while retaining the interference suppression of a narrow beamwidth antenna. The antenna is scanned by a mechanical actuation of the radiation elements or of an additional reflector element in azimuth or elevation. Typically, well-behaved radiation patterns can be obtained over the complete field of view without significant performance degradation.

5) Comparison: Table VI highlights the differences between the four previously described approaches.

While a mechanical scanning antenna allows a good coverage of any desired field of view for short- and long-range operation with high suppression of interferers or clutter, however it is typically complex to manufacture and the scanning speed is restricted. A combination with other concepts is not seen practical.

Quasi-optical beamforming allows to achieve a narrow antenna beam with high gain and is ideally suited for long-range operation. It can be very cost-effective to manufacture and also serve as radome. On the downside, it is not a very flexible concept, as the field of view is fixed by the quasi-optical element.

Analog beamforming allows the realization of a very flexible antenna system with high performance and requires almost no additional signal processing power, as the beam steering is done in the millimeter-wave frontend. However the practical implementation proves difficult. To achieve good performance, a large number of channels are necessary. The challenges are then the number of interconnects to the active circuits, routing of the many channels, isolation between the channels and calibration of the antenna system.

Digital beamforming shows a lot of promise, allowing a flexible antenna system with high performance. However, a practical implementation leads to some of the same challenges as for analog beamforming. Additionally, the digital signal processing in the baseband requires more processing power compared to other concepts.

Hybrid systems, combining the different approaches to avoid the disadvantages of one individual concept alone can be envisioned. For example, to improve interference suppression and reduce the number of required channels of a digital

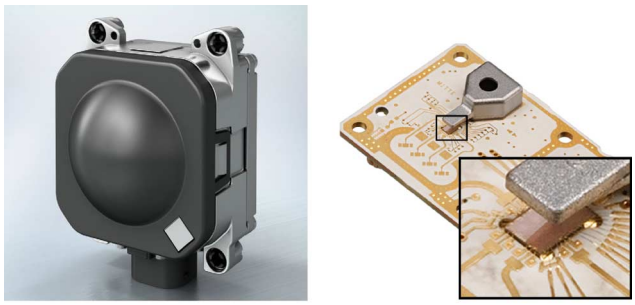

(a) (b)

Fig. 17. Bosch LRR3 sensor. (a) Sensor housing, (b) Topside of RF PCB module.

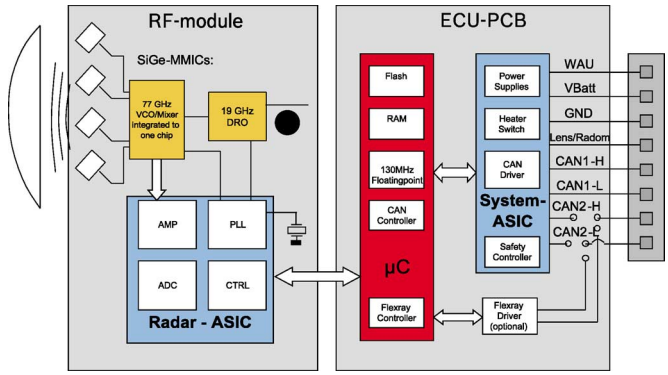

Fig. 18. Block diagram of LRR3 sensor.

beamforming concept, a quasi-optical beamforming network can be added to define the field of view without degrading the advantages of the DBF system. Such a hybrid antenna can fulfill the requirements of a high performance antenna system as well as the requirements of low-cost, compact and robust radar sensor. For example, a hybrid array that employs phased array and digital beamforming concepts that allow the advantages of both systems to be realized in the same architecture [87]–[89].

V. Examples

After presenting current and future active components, their packaging as well as various antenna concepts, in this section three specific sensor examples will be introduced. Starting with a state-of-the-art long range sensor and a mid range sensor currently under development, finally an Antenna on Chip demonstrator is presented, giving an outlook on upcoming trends for automotive radar.

A. Long Range Radar

Fig. 17(a) illustrates Bosch's current long range sensor LRR3, which has already been introduced in Section II.C. It consists of a lens antenna, diecast housing, car connector, 77 GHz transceiver module, ECU board and diecast back side cover. The lens antenna [73] is clipped and bonded to the diecast housing. From the bottom side, the transceiver module is placed in a cavity and screwed on the housing in a way that the antennas can radiate through an opening in the middle. Subsequently, the ECU board is attached to the car connector and to the transceiver board using a board-to-board connector. Both PCBs are secured by the diecast cover comprising structures for heat dissipation and a pressure equalization element. At the end of the assembly line, the deviation between the radar axis and the sensor's mechanical axis is measured and stored in the sensor unit for alignment procedures at the car manufacturer.

A simplified block diagram of the sensor is depicted in Fig. 18. The major innovations in comparison to its predecessor LRR2 are to be found in size and package complexity reduction of the RF module by implementing SiGe MMICs instead of Gunn oscillators and discrete mixer diodes (see Fig. 17(b)). The transceiver chip as presented in Section IV-A.2 and the reference DRO MMIC are placed in cavities using CoB packaging (see Section 8) to accomplish short bond wires and to improve their heat dissipation due to a 300 μm strong copper layer below. The reference MMIC contains a 19 GHz oscillator, stabilized by an external ceramic resonator being frequency adjusted accurately by a laser trimming process [11]. Reference signal and LO signal being divided by four are mixed and after passing additional dividers fed into a phased locked loop (PLL) to circumvent the fact that high divide ratios tremendously increase the in-loop phase noise and thus degrade the dynamic range [90].

Subsequently, the signal is split and transmitted to the four patch antennas, which are rotated by 45° in order to be less prone to inferring millimeter-wave radiation. Each patch structure consists of the actual directly excited patch and two parasitic patches to increase the bandwidth to 4 GHz and to generate narrower beams. The resulting two-way antenna diagram is illustrated in Fig. 19, showing the squint between all four beams being used for angle estimation. After down-converting, the receive signals are amplified, filtered and A/D converted by an ASIC located on the backside of the RF module and being furthermore responsible for modulation and power control, sequencing and diagnostics. Subsequent signal processing is then carried out on the μC of the ECU board.

B. Mid Range Radar

To illustrate the progress since the development of third generation radar sensors, subsequently a new mid range radar sensor, called MRR is presented. This sensor, announced in 2011, is in contrast to precedent sensor generations a bistatic system, and like for all generations before its development is strongly driven by innovations of the transceiver unit. The sensor housing and the RF frontend PCB are shown in Fig. 20(a). The block diagram Fig. 21 depicts the bistatic setup of the radar. The transmitter chip feeds a multi-column transmit patch array and provides the LO signal for the receiver chip. The receiver features four channels, which are fed by individual patch columns.

The bonded 77 GHz and 19 GHz MMICs are replaced by a transmit SiGe MMIC, similar to the one mentioned in Section IV-A.2 and its counterpart for the receive path, being both packaged in eWLB technology (see Section IV-B.3) to benefit from state-of-the-art "Pick&Place" processes and from better RF performance [91], [92]. Subsequent processing is again carried out using an ASIC and a μC. Instead of a combination of antenna patches and a dielectric lens, planar antennas are used comprising four receive and two transmit channels.

The according transmit antennas and a close up view of the receiver MMIC are illustrated in Fig. 20(b). The main transmit

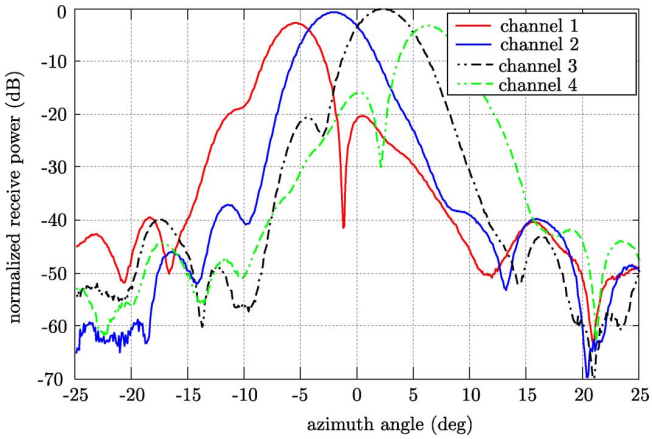

Fig. 19. Two-way antenna diagram of LRR3.

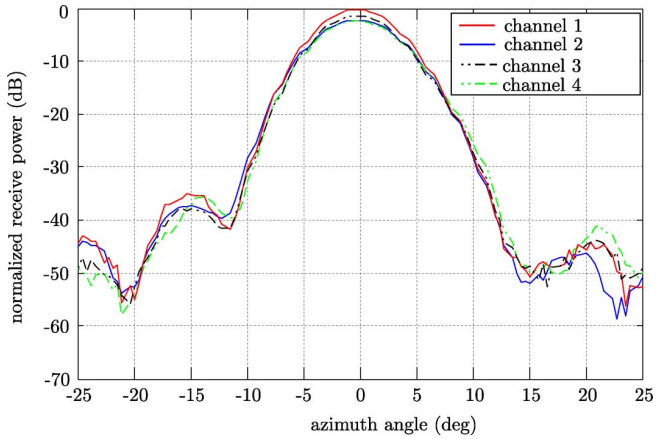

Fig. 22. Two-way antenna diagram for the front-side MRR sensor.

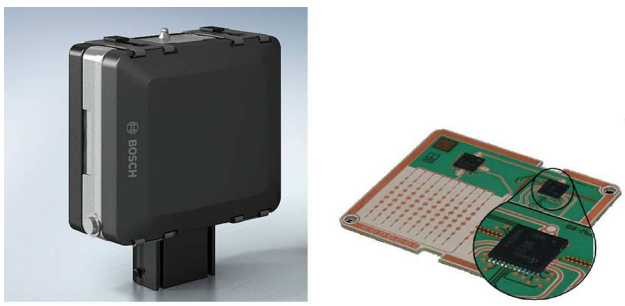

Fig. 20. Bosch MRR sensor. (a) Sensor housing, (b) RF PCB module with planar antenna.

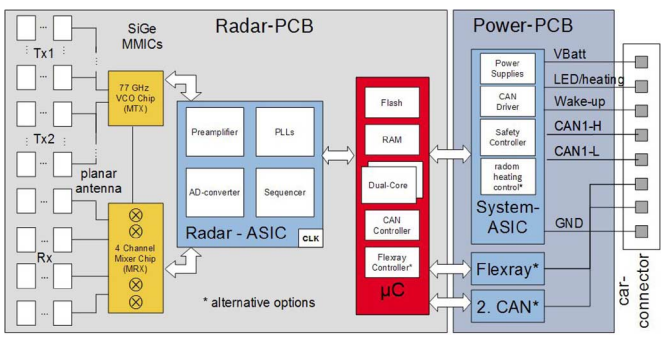

Fig. 21. Block diagram of the MRR sensor.

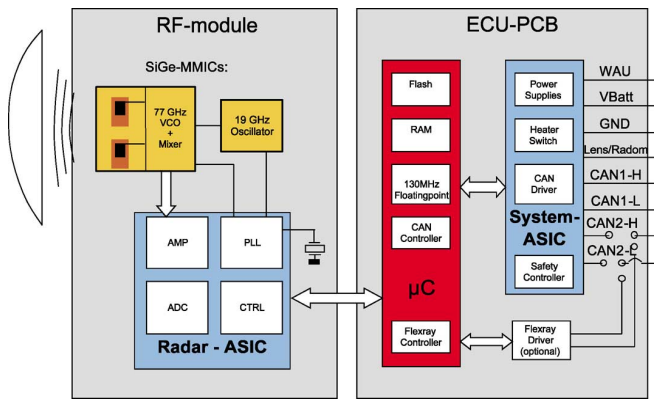

Fig. 23. Block diagram of the radar sensor with on-chip antenna.

array consists of ten columns and achieves a sidelobe level suppression of better than 30 dB. The field of view can be broadened by using an additional single-column transmit channel. The losses of the microstrip feed lines are in the order of 0.8 dB/cm. They do not impact the overall sensor performance, as sufficient system dynamic is available for midrange operation. Fabrication variations in the permittivity of the PCB only slightly influence the antenna characteristics. On the other hand, the unidirectional feeding of the antenna elements causes a tilt of the main lobe when changing the transmit frequency. Therefore, the array is designed to minimize this effect within the bandwidth of 1 GHz around the center frequency.

The planar antenna array can be easily modified to realize different antenna patterns for front and rear/side car integration. The two-way antenna diagram for the four different receive channels, using frontside transmit antenna characteristics, is depicted in Fig. 22.

C. Antenna on Chip Demonstrator

To demonstrate the performance of the on-chip antenna concept, presented in Section IV-B.5, a complete radar sensor was built based on the LRR3 sensor [93]. Only the top side with the RF substrate of the LRR3 RF module has been replaced with the QFN packaged transceiver introduced in Section IV-B.5, all other modules remain identical.

The PCB surrounding the QFN package contains all additional electronic components to control this 19 GHz VCO. A standard integer PLL was used to stabilize the 19 GHz VCO, using the divider by 8 from the MMIC. A 10 MHz quartz is used as a reference for the PLL. All of the remaining PLL and baseband circuits remain identical to the LRR3 radar sensor.

The fabricated RF module PCB is shown in Fig. 24(b). The SiGe radar transceiver can be seen mounted inside the QFN package on the middle of the board. The stabilization PLL and quartz reference are placed next to the QFN package.

Fig. 24(a) shows the complete radar sensor integrated in the sensor housing with the unmounted LRR3 dielectric lens. The housing, used for LRR3, was slightly adapted and absorber material was used to suppress unwanted reflections between the metal housing and dielectric lens antenna. The two antenna elements were mounted nearly in the identical position as the LRR3 antenna feed patches.

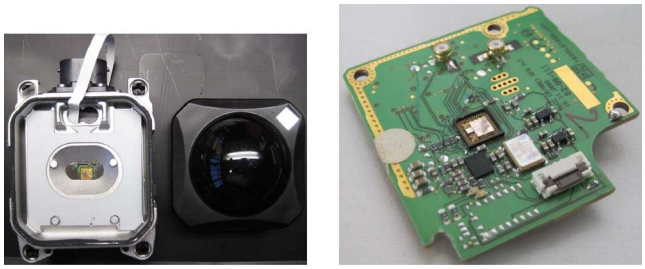

(a) (b)

Fig. 24. Antenna on-chip demonstrator. (a) LRR3 sensor housing, (b) PCB module with QFN package containing antenna on-chip.

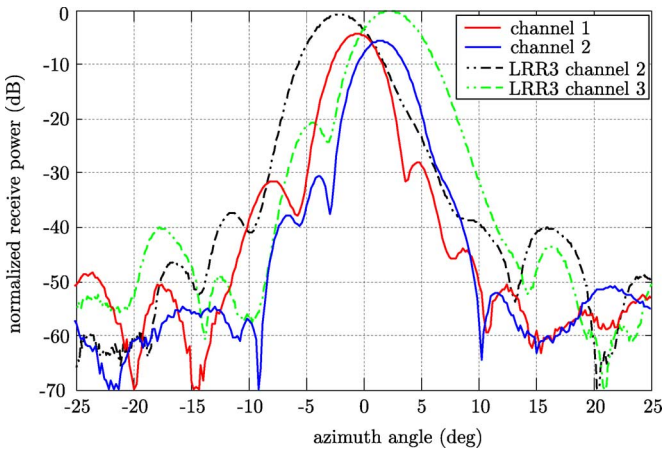

Fig. 25. Two-way antenna diagram of the antenna on chip demonstrator compared to an LRR3.

To verify the performance of the sensor, two way response measurements of the two monostatic radar channels were performed by operating the sensor using FMCW modulation and placing a corner reflector in a distance of several meters. The received power reflected from the corner reflector is recorded at the baseband after amplification, filtering, analog to digital conversion and signal processing by using fast fourier transformation.

This setup allows a direct comparison with a LRR3 sensor. Fig. 25 shows a two-way antenna pattern in the azimuthal plane of two on-chip antennas and two channels of the LRR3 from Fig. 19. A 3 dB difference in peak values of received powers between LRR3 and Antenna on Chip demonstrator is observed after the measurements. A mismatch in the illumination of the dielectric lens by the on-chip antennas and broader beamwidth of the on-chip patch antennas compared to the beamwidth of the LRR3 patch feeds are the reasons for this amplitude difference.

The placement of the on-chip antennas on the transceiver chip was not optimized. Taking into account the 2–3 mm long on-chip microstrip feed lines leading to the antenna elements with a loss of 1 dB/mm, the sensor performance can be optimized to exceed the LRR3 reference sensor for at least 3 dB.

VI. Conclusion

An overview of the key issues in semiconductor technology, packaging and antenna systems for millimeter-wave technology used in automotive radar sensors was provided. Advanced packaging concepts and antenna systems are explained in detail and evaluated. The presented measurement results of the radar frontends demonstrate their good performance.

On the semiconductor side, several manufacturers are able to provide modern processes with sufficient performance. SiGe BiCMOS technology was identified as the currently most promising semiconductor technology for low-cost millimeter-wave radar sensors.

A number of packaging technologies to interconnect the semiconductor chip with a PCB have been introduced. Starting with well known chip on board wire bonding and flip-chip mounting, a number of newer developments were presented to achieve lower cost solutions. The eWLB package allows soldering 77 GHz as standard SMD components, drastically reducing production efforts. By integrating the antenna in the package itself, a solution to eliminate expensive millimeter-wave capable substrate was shown. Taking this approach even one step further, an antenna on chip concept was presented, showing very good performance, comparable to off-chip approaches.

The selection of the antenna system has been addressed by introducing and comparing four different concepts. The comparison shows that a hybrid system, combining different concepts, is a promising way to implement the antenna system for an automotive radar system. Especially extending digital beamforming with approaches like analog or quasi-optical beamforming can deliver a flexible and competitive solution.

Finally three different realizations of automotive radar sensors were introduced, showing the path from current to next to future generation implementations.

Acknowledgment

The authors would like to thank Infineon for providing the millimeter-wave integrated circuits.

References

[1] R. Adomat, G.-O. Geduld, M. Schamberger, and P. Rieth, "Advanced driver assistance systems for increased comfort and safety—Current developments and an outlook to the future on the road," *Avd. Microsyst. Autom. Appl.*, pp. 431–446, 2003.

[2] M. van Schijndel-de Nooij, A. Schieben, N. Ford, and M. McDonald, "Definition of necessary vehicle and infrastructure systems for automated driving," European Commission, Information Society and Media DG, Components and Systems Directorate - ICT for Transport, Study Rep. SMART 2010/0064, Jun. 2011.

[3] R. H. Rasshofer and K. Gresser, "Automotive radar and lidar systems for next generation driver assistance functions," *Adv. Radio Sci.*, vol. 3, pp. 205–209, 2005.

[4] S. K. P. Zador and R. Vocas, "Final Report-Automotive Collision Avoidance (ACAS) Program," Tech. Rep. DOT HS 809 080, NHTSA, U.S. DOT, Aug. 2000.

[5] R. Altendorfer, S. Wirkert, and S. Heinrichs-Bartscher, "Sensor fusion as an enabling technology for safety-critical driver assistance systems," *SAE Int. J. Passeng. Cars—Electron. Electr. Syst.*, vol. 3, pp. 183–192, Dec. 2010.

[6] J. Wenger, "Automotive radar—Status and perspectives," in *Proc. IEEE Compound Semicond. Integr. Circuit Symp.*, Oct. 2005, pp. 21–25.

[7] "Report on Interference Density Increase by Market Penetration Forecast," Mosarim Project, D1.6, 2010 [Online]. Available: http://www.mosarim.eu/

[8] F. Pfeiffer and E. Biebl, "Inductive compensation of high-permittivity coatings on automobile long-range radar radomes," *IEEE Trans. Microw. Theory Tech.*, vol. 57, no. 11, pp. 2627–2632, Nov. 2009.

[9] European Telecommunications Standards Institute, *EN 302 264-1:* Electromagnetic Compatibility and Radio Spectrum.

[10] Federal Communications Commission, FCC 11-79 May 2011.

[11] D. Freundt and B. Lucas, "Long range radar sensor for high-volume driver assistance systems market," in *Proc. SAE World Congress & Exhibition*, 2008, pp. 117–124.

[12] W. Menzel, "Millimeter-wave radar for civil applications," in *Proc. Eur. Radar Conf.*, Oct. 2010, pp. 89–92.

[13] V. Manasson, L. Sadovnik, and R. Mino, "MMW scanning antenna," *IEEE Aerosp. Electron. Syst. Mag.*, vol. 11, no. 10, pp. 29–33, Oct. 1996.

[14] H. Mizuno, N. Tomioka, A. Kawakubo, and T. Kawasaki, "A forward-looking sensing millimeter-wave radar," in *Proc. JSAE Ann. Congr.*, 2004, no. 33-04, pp. 5–8.

[15] H.-L. Bloecher and J. Dickmann, "Automotive radar for safety and driver assistance applications: Status and trends," presented at the Eur. Radar Conf. Workshop WFF01, Oct. 2010.

[16] S. Buckley, "Radar based driver assistance features," presented at the IWPC—Autom. Radar Workshop, Feb. 2011.

[17] M. I. Skolnik, *Introduction to Radar Systems*. New York: McGraw-Hill, 2001.

[18] H. Buddendick and T. Eibert, "Acceleration of ray-based radar cross section predictions using monostatic-bistatic equivalence," *IEEE Trans. Antennas Propag.*, vol. 58, no. 2, pp. 531–539, Feb. 2010.

[19] L. Mesow, "Multisensorielle datensimulation im fahrzeugumfeld für die bewertung von sensorfusionsalgorithmen," Ph.D. dissertation, Technical Univ. Chemnitz, Germany, 2007.

[20] M. Bühren and B. Yang, "Automotive radar target list simulation based on reflection center representation of objects," in *Proc. Workshop Intell. Transport. (WIT)*, Hamburg, Germany, Mar. 2006, pp. 161–166.

[21] G. R. Curry, *Radar System Performance Modeling*. Norwood, MA: Artech House, 2005.

[22] Y. Liu, D. Goshi, K. Mai, L. Bui, and Y. Shih, "Linearity study of DDSbased W-band FMCW sensor," in *Proc. IEEE MTT-S Int. Microw. Symp. Dig.*, Jun. 2009, pp. 1697–1700.

[23] E. Hecht, *Optics*, 4th ed. New York: Addison Wesley, 2001.

[24] I. Gresham, N. Jain, T. Budka, A. Alexanian, N. Kinayman, B. Ziegner, S. Brown, and P. Staecker, "A compact manufacturable 76–77-GHz radar module for commercial ACC applications," *IEEE Trans. Microw. Theory Tech.*, vol. 49, no. 1, pp. 44–58, Jan. 2001.

[25] P. Alleaume, C. Toussain, C. Auvinet, D. Domnesque, P. Quentin, and M. Camiade, "Millimetre-wave hot-via interconnect-based GaAs chipset for automotive RADAR and security sensors," in *Proc. Eur. Microw. Integr. Circuit Conf.*, Oct. 2008, pp. 52–55.

[26] G. Brehm, "Trends in microwave/millimeter-wave front-end technology," presented at the EuMIC, Sep. 2006.

[27] D. Platt, L. Pettersson, D. Jakonis, M. Salter, and J. Hagglund, "Integrated 79 GHz UWB automotive radar front-end based on hi-mission MCM-D silicon platform," in *Proc. Eur. Radar Conf.*, Oct. 2009, pp. 445–448.

[28] T. Nagasaku, K. Kogo, H. Shinoda, H. Kondoh, Y. Muto, A. Yamamoto, and T. Yoshikawa, "77 GHz low-cost single-chip radar sensor for automotive ground speed detection," presented at the IEEE Compound Semicond. Integr. Circuit Symp., Oct. 2008.

[29] K. Kim, W. Choi, S. Kim, G. Seol, K. Seo, and Y. Kwon, "A 77 GHz transceiver for automotive radar system using a 120 nm In0.4AlAs/In0.35GaAs metamorphic HEMTs," in *Proc. IEEE Compound Semicond. Integr. Circuit Symp.*, Nov. 2006, pp. 201–204.

[30] S. Nicolson, K. Tang, K. Yau, P. Chevalier, B. Sautreuil, and S. Voinigescu, "A low-voltage 77-GHz automotive radar chipset," in *Proc. IEEE MTT-S Int. Microw. Symp. Dig.*, Jun. 2007, pp. 487–490.

[31] L. Wang, S. Glisic, J. Borngraeber, W. Winkler, and J. Scheytt, "A single-ended fully integrated SiGe 77/79 GHz receiver for automotive radar," *IEEE J. Solid-State Circuits*, vol. 43, no. 9, pp. 1897–1908, Sep. 2008.

[32] A. Babakhani, X. Guan, A. Komijani, A. Natarajan, and A. Hajimiri, "A 77-GHz phased-array transceiver with on-chip antennas in silicon: Receiver and antennas," *IEEE J. Solid-State Circuits*, vol. 41, no. 12, pp. 2795–2806, Dec. 2006.

[33] W. Huang, J. John, S. Braithwaite, J. Kirchgessner, I. Lim, D. Morgan, Y. Park, S. Shams, I. To, P. Welch, R. Reuter, H. Li, A. Ghazinour, P. Wennekers, and Y. Yin, "SiGe 77 GHz automotive radar technology," in *Proc. IEEE Int. Symp. Circuits Syst.*, May 2007, pp. 1967–1970.

[34] A. Kar-Roy, D. Howard, E. Preisler, M. Racanelli, S. Chaudhry, and V. Blaschke, "SiGe BiCMOS manufacturing platform for mmWave applications," in *Proc. Society Photo-Optical Instrumentation Engineers (SPIE) Conf. Ser.*, Oct. 2010, vol. 7837.

[35] G. Avenier, M. Diop, P. Chevalier, G. Troillard, N. Loubet, J. Bouvier, L. Depoyan, N. Derrier, M. Buczko, C. Leyris, S. Boret, S. Montusclat, A. Margain, S. Pruvost, S. Nicolson, K. Yau, N. Revil, D. Gloria, D. Dutartre, S. Voinigescu, and A. Chantre, "0.13 SiGe BiCMOS technology fully dedicated to mm-Wave applications," *IEEE J. Solid-State Circuits*, vol. 44, no. 9, pp. 2312–2321, Sep. 2009.

[36] J.-S. Rieh, B. Jagannathan, H. Chen, K. Schonenberg, D. Angell, A. Chinthakindi, J. Florkey, F. Golan, D. Greenberg, S.-J. Jeng, M. Khater, F. Pagette, C. Schnabel, P. Smith, A. Stricker, K. Vaed, R. Volant, D. Ahlgren, G. Freeman, K. Stein, and S. Subbanna, "SiGe HBTs with cut-off frequency of 350 GHz," in *Proc. Int. Electron Devices Meeting*, Dec. 2002, pp. 771–774.

[37] J. Bock, H. Schafer, K. Aufinger, R. Stengl, S. Boguth, R. Schreiter, M. Rest, H. Knapp, M. Wurzer, W. Perndl, T. Bottner, and T. Meister, "SiGe bipolar technology for automotive radar applications," in *Proc. Bipolar/BiCMOS Circuits Technol. Meeting*, Sep. 2004, pp. 84–87.

[38] H. Forstner, H. Knapp, H. Jager, E. Kolmhofer, J. Platz, F. Starzer, M. Treml, A. Schinko, G. Birschkus, J. Bock, K. Aufinger, R. Lachner, T. Meister, H. Schafer, D. Lukashevich, S. Boguth, A. Fischer, F. Reininger, L. Maurer, J. Minichshofer, and D. Steinbuch, "A 77 GHz 4-channel automotive radar transceiver in SiGe," in *Proc. IEEE Radio Freq. Integr. Circuits (RFIC) Symp.*, Jun. 2008, pp. 233–236.

[39] S. Trotta, H. Li, B. Dehlink, A. Ghazinour, Y. Yin, R. Reuter, S. Majied, and J. John, "A transceiver chipset for automotive LRR and SRR systems in the 76–77 and 77–81 GHz bands in SiGe BiCMOS technology," in *Proc. IEEE Radio Freq. Integr. Circuits (RFIC) Symp.*, Jun. 2011.

[40] J. Cressler, "On the potential of SiGe HBTs for extreme environment electronics," *Proc. IEEE*, vol. 93, no. 9, pp. 1559–1582, Sep. 2005.

[41] F. Ellinger, *Radio Frequency Integrated Circuits and Technologies*. New York: Springer, 2008.

[42] S. Nicolson, P. Chevalier, B. Sautreuil, and S. Voinigescu, "Single-chip W-band SiGe HBT transceivers and receivers for Doppler radar and millimeter-wave imaging," *IEEE J. Solid-State Circuits*, vol. 43, no. 10, pp. 2206–2217, Oct. 2008.

[43] T. Mitomo, N. Ono, H. Hoshino, Y. Yoshihara, O. Watanabe, and I. Seto, "A 77 GHz 90 nm CMOS transceiver for FMCW radar applications," *IEEE J. Solid-State Circuits*, vol. 45, no. 4, pp. 928–937, Apr. 2010.

[44] Y. Kawano, T. Suzuki, M. Sato, T. Hirose, and K. Joshin, "A 77 GHz transceiver in 90 nm CMOS," in *Proc. IEEE Solid-State Circuits Conf.*, Feb. 2009, pp. 310, 311a–311.

[45] Y.-A. Li, M.-H. Hung, S.-J. Huang, and J. Lee, "A fully integrated 77 GHz FMCW radar system in 65 nm CMOS," in *Proc. IEEE Solid-State Circuits Conf.*, Feb. 2010, pp. 216–217.

[46] A. Margomenos, "A comparison of Si CMOS and SiGe BiCMOS technologies for automotive radars," presented at the IEEE Topical Meeting Silicon Monolithic Integr. Circuits RF Syst., 2009.

[47] J.-J. Lin, K.-H. To, D. Hammock, B. Knappenberger, M. Majerus, and W. Huang, "Power amplifier for 77-GHz automotive radar in 90-nm LP CMOS technology," *IEEE Microw. Wireless Compon. Lett.*, vol. 20, no. 5, pp. 292–294, May 2010.

[48] J. Scholvin, D. R. Greenberg, and J. A. del Alamo, "Fundamental power and frequency limits of deeply-scaled CMOS for RF power applications," presented at the Int. Electron Devices Meeting, Dec. 2006.

[49] M. Chang, "Foundry future: Challenges in the 21st century," in *Proc. IEEE Solid-State Circuits Conf.*, Feb. 2007, pp. 18–23.

[50] "International Technology Roadmap for Semiconductors (ITRS),", Millimeter Wave 10 GHz–100 GHz Technology Requirements 2010 [Online]. Available: http://www.itrs.net

[51] P. Chevalier, F. Pourchon, T. Lacave, G. Avenier, Y. Campidelli, L. Depoyan, G. Troillard, M. Buczko, D. Gloria, D. Celi, C. Gaquiere, and A. Chantre, "A conventional double-polysilicon FSA-SEG Si/SiGe:C HBT reaching 400 GHz fMAX," in *Proc. Bipolar/BiCMOS Circuits Technol. Meeting*, Oct. 2009.

[52] W. Perndl, H. Knapp, M. Wurzer, K. Aufinger, T. Meister, T. Bock, W. Simburger, and A. Scholtz, "A low-noise, and high-gain double-balanced mixer for 77 GHz automotive radar front-ends in SiGe bipolar technology," in *Proc. IEEE Radio Freq. Integr. Circuits (RFIC) Symp.*, Jun. 2004, pp. 47–50.

[53] S. Yang, H. Forstner, G. Haider, H. Kainmueller, K. Aufinger, L. Maurer, and R. Hagelauer, "A low noise, high gain, highly linear mixer for 77 GHz automotive radar applications in SiGe:C bipolar technology," in *Proc. ESSCIRC*, Sep. 2009, pp. 312–315.

[54] M. Steinhauer, "Digital beamforming-konzepte," Ph.D. dissertation, Univ. Ulm, Germany, 2006.

[55] H. P. Forstner, H. D. Wohlmuth, H. Knapp, C. Gamsjaeger, J. Boeck, T. Meister, and K. Aufinger, "A 19 GHz DRO downconverter MMIC for 77 GHz automotive radar frontends in a SiGe bipolar production technology," in *Proc. Bipolar/BiCMOS Circuits Technol. Meeting*, 2008.
[56] O. Günther, "Modellierung und Leakage-Kompensation von 77 GHz FMCW-Weitbereichsradar-Transceivern in SiGe-Technologie für Kfz-Anwendungen," Ph.D. dissertation, Univ. Erlangen, Germany, 2008.
[57] K. Kuang, F. Kim, and S. S. Cahill, *RF and Microwave Microelectronics Packaging*. New York: Springer, 2010.
[58] T. Budka, "Wide-bandwidth millimeter-wave bond-wire interconnects," *IEEE Trans. Microw. Theory Tech.*, vol. 49, no. 4, pp. 715–718, Apr. 2001.
[59] W. Heinrich, "The flip-chip approach for millimeter wave packaging," *IEEE Microw. Mag.*, vol. 6, no. 3, pp. 36–45, Sep. 2005.
[60] A. Jentzsch and W. Heinrich, "Theory and measurements of flip-chip interconnects for frequencies up to 100 GHz," *IEEE Trans. Microw. Theory Tech.*, vol. 49, no. 5, pp. 871–878, May 2001.
[61] M. Brunnbauer, E. Furgut, G. Beer, T. Meyer, H. Hedler, J. Belonio, E. Nomura, K. Kiuchi, and K. Kobayashi, "An embedded device technology based on a molded reconfigured wafer," in *Proc. Electron. Compon. Technol. Conf.*, Jul. 2006, pp. 547–551.
[62] M. Wojnowski, M. Engl, M. Brunnbauer, K. Pressel, G. Sommer, and R. Weigel, "High frequency characterization of thin-film redistribution layers for embedded wafer level BGA," in *Proc. Electron. Packag. Technol. Conf.*, Dec. 2007, pp. 308–314.
[63] M. Wojnowski, M. Engl, B. Dehlink, G. Sommer, M. Brunnbauer, K. Pressel, and R. Weigel, "A 77 GHz SiGe mixer in an embedded wafer level BGA package," in *Proc. Electron. Compon. Technol. Conf.*, May 2008, pp. 290–296.
[64] T. Meyer, K. Pressel, G. Ofner, and B. Römer, "System integration with eWLB," presented at the Electron. Syst.-Integr. Technol. Conf. (ESTC), Sep. 2010.
[65] M. Brunnbauer, T. Meyer, G. Ofner, K. Mueller, and R. Hagen, "Embedded wafer level ball grid array (eWLB)," in *Proc. Electron. Manuf. Technol. Symp.*, Nov. 2008, pp. 994–998.
[66] S. W. Yoon, A. Bahr, X. Baraton, P. Marimuthu, and F. Carson, "3D eWLB (embedded wafer level BGA) technology for 3D-packaging/3D-SiP (systems-in-package) applications," in *Proc. Electron. Packag. Technol. Conf.*, Dec. 2009, pp. 915–919.
[67] M. Al Henawy and M. Schneider, "Integrated antennas in eWLB packages for 77 GHz and 79 GHz automotive radar sensors," in *Proc. Eur. Microw. Conf.*, Oct. 2011, pp. 424–427.
[68] R. Carrillo-Ramirez and R. Jackson, "A highly integrated millimeter-wave active antenna array using BCB and silicon substrate," *IEEE Trans. Microw. Theory Tech.*, vol. 52, no. 6, pp. 1648–1653, Jun. 2004.
[69] I. Papapolymerou, R. F. Drayton, and L. Katehi, "Micromachined patch antennas," *IEEE Trans. Antennas Propag.*, vol. 46, no. 2, pp. 275–283, Feb. 1998.
[70] J. Hasch, U. Wostradowski, S. Gaier, and T. Hansen, "77 GHz radar transceiver with dual integrated antenna elements," in *Proc. German Microw. Conf.*, Mar. 2010, pp. 280–283.
[71] Y. Atesal, B. Cetinoneri, M. Chang, R. Alhalabi, and G. Rebeiz, "Millimeter-wave wafer-scale silicon BiCMOS power amplifiers using free-space power combining," *IEEE Trans. Microw. Theory Tech.*, vol. 59, no. 4, pp. 954–965, Apr. 2011.
[72] H. P. Forstner, H. Knapp, C. Gamsjaeger, H. Rein, J. Boeck, T. Meister, and K. Aufinger, "A 19 GHz VCO downconverter MMIC for 77 GHz automotive radar frontends in a SiGe bipolar production technology," in *Proc. Eur. Microw. Conf.*, 2007, pp. 178–181.
[73] T. Binzer, M. Klar, and V. Gross, "Development of 77 GHz radar lens antennas for automotive applications based on given requirements," in *Proc. ITG Conf. Antennas*, Mar. 2007, pp. 205–209.
[74] W. Menzel, D. Pilz, and R. Leberer, "A 77 GHz FM/CW radar frontend with a low-profile, low-loss printed antenna," in *Proc. IEEE MTT-S Int. Microw. Symp. Dig.*, Jun. 1999, pp. 1485–1488.
[75] D. Chouvaev and M. Danestig, "Slot antennas and quasi-optical beamforming for a cost-efficient integrated automotive radar," presented at the GigaHertz Symp., Linköping, Sweden, 2003.
[76] G. Kühnle, H. Mayer, H. Olbrich, W. Steffens, and H.-C. Swoboda, "Low-cost long-range radar for future driver assistance systems," *Auto Technol.*, vol. 4, pp. 76–79, 2003.
[77] M. Steinhauer, H.-O. Ruo, H. Irion, and W. Menzel, "Millimeter-wave-radar sensor based on a transceiver array for automotive applications," *IEEE Trans. Microw. Theory Tech.*, vol. 56, no. 2, pp. 261–269, Feb. 2008.
[78] Y. Asano, S. Ohshima, T. Harada, M. Ogawa, and K. Nishikawa, "Proposal of millimeter-wave holographic radar with antenna switching," in *Proc. IEEE MTT-S Int. Microw. Symp. Dig.*, vol. 2, pp. 1111–1114.
[79] C. Lievers, W. van Rossum, A. Maas, and A. Huizing, "Digital beam forming on transmit and receive with an AESA FMCW radar," in *Proc. Eur. Radar Conf.*, Oct. 2007, pp. 47–50.
[80] S. Holzwarth, O. Litschke, W. Simon, K. Kuhlmannt, and A. F. Jacob, "Far field pattern analysis and measurement of a digital beam forming 8×8 antenna array transmitting from 29.5 to 30 GHz," presented at the Eur. Conf. Antennas Propag., Nov. 2007.
[81] I. Sarkas, M. Khanpour, A. Tomkins, P. Chevalier, P. Garcia, and S. Voinigescu, "W-band 65-nm CMOS and SiGe BiCMOS transmitter and receiver with lumped I-Q phase shifters," in *Proc. IEEE Radio Freq. Integr. Circuits (RFIC) Symp.*, Jun. 2009, pp. 441–444.
[82] C. Wagner, M. Hartmann, A. Stelzer, and H. Jaeger, "A fully differential 77 GHz active IQ modulator in a silicon-germanium technology," *IEEE Microw. Wireless Compon. Lett.*, vol. 18, pp. 362–364, May 2008.
[83] A. M. Niknejad and H. Hashemi, *mm-Wave Silicon Technology: 60 GHz and Beyond*. New York: Springer, 2007.
[84] G. Rebeiz and K. Koh, "Silicon RFICs for phased arrays," *IEEE Microw. Mag.*, vol. 10, no. 3, pp. 96–103, May 2009.
[85] A. Natarajan, A. Komijani, X. Guan, A. Babakhani, and A. Hajimiri, "A 77-GHz phased-array transceiver with on-chip antennas in silicon: Transmitter and local LO-path phase shifting," *IEEE J. Solid-State Circuits*, vol. 41, no. 12, pp. 2807–2819, Dec. 2006.
[86] D. Parker and D. Zimmermann, "Phased Arrays—Part II: Implementations, applications, and future trends," *IEEE Trans. Microw. Theory Tech.*, vol. 50, no. 3, pp. 688–698, Mar. 2002.
[87] S. Tokoro, K. Kuroda, A. Kawakubo, K. Fujita, and H. Fujinami, "Electronically scanned millimeter-wave radar for pre-crash safety and adaptive cruise control system," in *Proc. Intell. Veh. Symp.*, Jun. 2003, pp. 304–309.
[88] L. Baggen, S. Holzwarth, M. Boettcher, and M. Eube, "Advances in phased array technology," in *Proc. Eur. Radar Conf.*, Sep. 2006, pp. 88–91.
[89] F. van Vliet and A. de Hek, "Front-end technology for phased-arrays with digital beamforming," presented at the Conf. Microw., Commun., Antennas Electron. Syst., May 2008.
[90] C. Wagner, A. Stelzer, and H. Jager, "PLL architecture for 77-GHz FMCW radar systems with highly-linear ultra-wideband frequency sweeps," in *Proc. IEEE MTT-S Int. Microw. Symp. Dig.*, Jun. 2006, pp. 399–402.
[91] J. Hildebrandt, "77 GHz mid range radar for a variety of applications," presented at the IWPC—Automotive Radar Workshop, Feb. 2011.
[92] P. Tamang, "Radar sensors," *Vision Zero Int.*, pp. 68–69, Jun. 2011 [Online]. Available: http://www.scribd.com/doc/58141328/Vision-Zero-International-June-2011
[93] J. Hasch, U. Wostradowski, R. Hellinger, and D. Mittelstrass, "77 GHz automotive radar sensor in low-cost PCB technology," in *Proc. Eur. Microw. Conf.*, Oct. 2011, pp. 101–104.

Jürgen Hasch was born in Göppingen, Germany, in 1970. He received the Dipl.-Ing. degree in 1996 and the Ph.D. degree in 2007 from the University of Stuttgart, Stuttgart, Germany.

He is a senior RF expert at corporate research of the Robert Bosch GmbH in Stuttgart, Germany. His main interests are ultrawideband and millimeter-wave sensors.

Dr. Hasch is a member of the IEEE Antennas and Propagation Society and the IEEE Microwave Theory and Techniques Society.

Eray Topak was born in Denizli, Turkey, in 1983. He received the M.Sc. degree in 2008 from the Technical University of Munich, Munich. Germany. Currently he is pursuing the Ph.D. degree at corporate research of the Robert Bosch GmbH, Stuttgart, Germany.

His main interests are millimeter-wave antenna systems.

Raik Schnabel was born in Weimar, Germany, in 1985. He received the Dipl.-Ing. degree in 2010 from the Karlsruhe Institute of Technology, Karlsruhe, Germany. Currently he is pursuing the Ph.D. degree at the business unit "Chassis Systems Control" of the Robert Bosch GmbH, Stuttgart, Germany.

His main interests are millimeter-wave integrated circuits.

Thomas Zwick (S'95–M'00–SM'06) received the Dipl.-Ing. (M.S.E.E.) and the Dr.-Ing. (Ph.D.E.E.) degrees from the Universität Karlsruhe (TH), Karlsruhe, Germany in 1994 and 1999, respectively.

From 1994 to 2001 he was Research Assistant at the Institut für Höchstfrequenztechnik und Elektronik (IHE), Universität Karlsruhe (TH), Germany. In February 2001, he joined IBM as a Research Staff Member at the IBM T. J. Watson Research Center, Yorktown Heights, NY. From October 2004 to September 2007, he was with Siemens AG, Lindau, Germany. During this period he managed the RF development team for automotive radars. In October 2007 he became appointed as Full Professor at the Karlsruhe Institute of Technology (KIT), Germany. He is Director of the Institut für Hochfrequenztechnik und Elektronik (IHE), KIT. His research topics include wave propagation, stochastic channel modeling, channel measurement techniques, material measurements, microwave techniques, millimeter wave antenna design, wireless communication and radar system design. He participated as an expert in the European COST231 *Evolution of Land Mobile Radio (Including Personal) Communications* and COST259 *Wireless Flexible Personalized Communications*. For the Carl Cranz Series for Scientific Education he served as a lecturer for *Wave Propagation*. He is the author or coauthor of over 100 technical papers and over 10 patents.

Dr. Zwick received the Best Paper Award on the International Symposium on Spread Spectrum Technology and Applications (ISSSTA 1998). In 2005 he received the Lewis Award for outstanding paper at the IEEE International Solid State Circuits Conference. Since 2008 he has been President of the Institute for Microwaves and Antennas (IMA).

Robert Weigel was born in Ebermannstadt, Germany, in 1956. He received the Dr.-Ing. and the Dr.-Ing.habil. degrees, both in electrical engineering and computer science, from the Munich University of Technology, Munich, Germany, in 1989 and 1992, respectively.

From 1982 to 1988, he was a Research Engineer, from 1988 to 1994 a Senior Research Engineer, and from 1994 to 1996 a Professor for RF Circuits and Systems at the Munich University of Technology. During 1994 to 1995 he was a Guest Professor for SAW Technology at Vienna University of Technology, Austria. From 1996 to 2002, he was Director of the Institute for Communications and Information Engineering at the University of Linz, Austria. In August 1999, he co-founded DICE—Danube Integrated Circuit Engineering, Linz, meanwhile split into an Infineon Technologies and an Intel company which are devoted to the design of RFICs. In 2000, he was appointed as Professor for RF Engineering at the Tongji University, Shanghai, China. Also in 2000, he co-founded the Linz Center of Competence in Mechatronics. Since 2002 he is Head of the Institute for Electronics Engineering at the University of Erlangen-Nuremberg. In 2009, he co-founded eesy-id, a company which is engaged with the design of medical electronic circuits and systems. He has been engaged in research and development of microwave theory and techniques, SAW technology, integrated optics, high-temperature superconductivity, digital and microwave communication and sensing systems, and automotive EMC. In these fields, he has published more than 750 papers and given about 300 international presentations. His review work includes international projects and journals.

Dr. Weigel received the German ITG Award in 2002 and the IEEE Microwave Applications Award in 2007. He serves on various editorial boards such as that of the Proceedings of the IEEE, and he has been editor of the Proceedings of the European Microwave Association (EuMA). He has been member of numerous conference steering and technical program committees. Currently he serves on several company and organization advisory boards in Europe and Asia. He is an elected scientific advisor of the German Research Foundation DFG. Within IEEE MTT-S, he has been Founding Chair of the Austrian COM/MTT Joint Chapter, Region 8 Coordinator and, during 2001 to 2003 Distinguished Microwave Lecturer, and currently he is an AdCom Member and Chair of MTT-2 Microwave Acoustics.

Christian Waldschmidt received the Dipl.-Ing. (M.S.E.E.) and the Dr.-Ing. (Ph.D.E.E.) degrees from the University Karlsruhe (TH), Karlsruhe, Germany, in 2001 and 2004, respectively.

From 2001 to 2004 he was a Research Assistant at the Institut für Höchstfrequenztechnik and Elektronik (IHE), Universität Karlsruhe (TH), Germany. Since 2004 he has been with Robert Bosch GmbH, in the business units Corporate Research and Chassis Systems. He was heading different research and development teams in high frequency engineering, EMC and automotive radar. His research topics include integrated radar sensors, radar system design, millimeter wave technologies, antennas and antenna arrays, UWB, and EMC. He is author or coauthor of over 50 technical papers and over 15 patents.